The Journal of Engineering Research Vol. 8 No. 1 (2011) 28-43

Effective Flange Width for Composite Steel Beams

T. Salama*[a] and H.H. Nassif[b]

*[a]*Civil, Construction and Environmental Engineering Department, University of Alabama at Birmingham, 1075 13th St. S., Birmingham, AL 35294-4440, USA*
*[b]*Civil and Environmental Engineering Department, Rutgers, The State University of New Jersey, 98 Brett Rd., 131 A-Wing, SOE Building, Piscataway, NJ 08854-8014, USA*

Received 30 March 2009; accepted 6 January 2010

العرض الفعال لشفة الكمرات الفولاذية المركبة

ت. سلامة * و هـ. هـ. نصيف

الخلاصة: تعتبر الشفة الفعالة من المبادئ المقترحة في المواصفات المختلفة لتبسيط حسابات توزيع الإجهاد بعرض الكمرات المركبة، وتم إثارة أسئلة حول صلاحية عرض البلاطة الفعال حيث له تأثير مباشر على حساب العزوم القصوى و كذلك حالة حد التشغيل مثل الالتواء، الاجهاد، و الأحمال الزائدة. وتقدم هذه الورقة نتائج إستقصاء تحليلي و معملي لتحديد العرض الفعال للشفة للكمرات الفولاذية المركبة، و تم إستخدام طريقة العناصر المحددة لتحليل كمرات خرسانية – فولاذية مركبة، بعروض مختلفة للشفة الخرسانية. و تم مقارنة النتائج مع نتائج ثمان كمرات بعروض مختلفه للشفة و درجات مختلفة من التاثير المركب (وصلات القص) و قد تم إختبارها حتى الانهيار. و قد بينت مقارنة الأحمال مع الإلتواء و الإنفعال في البلاطة الخرسانية أن مواصفات AISC-LRFD متحفظة و ينتج عنها عرض فعال قليل للشفة، وبناءا على دراسات بار امترية مفصلة أوصت النتائج بإستخدام معادلة لحساب العرض الفعال للشفة.

المفردات الممفتاحية : الكمرات الفولاذية المركبة، العرض الفعال للشفة، تحليل العناصر المحددة.

Abstract: The effective flange width is a concept proposed by various codes to simplify the computation of stress distribution across the width of composite beams. Questions have been raised as to the validity of the effective slab width provisions, since they have a direct effect on the computed ultimate moment as well as serviceability limit states such as deflection, fatigue, and overloading. The objective of this paper is to present results from an experimental and analytical investigation to determine the effective slab width in steel composite beams. The Finite Element Method (FEM) was employed for the analysis of composite steel-concrete beams having variable concrete flange widths. Results were compared to those from tests performed on eight beams loaded to failure. Beam test specimens had variable flange width and various degrees of composite action (shear connectors). The comparison presented in terms of the applied load versus deflection, and strain in the concrete slab show that the AISC-LRFD code is conservative and underestimates the width active. Based on a detailed parametric study an equation for the calculation of the effective flange width is recommended.

Keywords: composite steel beams; effective flange width; finite element analysis.

Nomenclature

A	Area of stress block
b_s	Width of concrete flange of composite beam
b_e	Effective width of concrete flange of composite beam
F	Area of steel plate
f_r	Fracture strength of concrete

*Corresponding author's email: talats@uab.edu

The Journal of Engineering Research Vol. 8 No. 1 (2011) 28-43

h Distance from mean plane of plate to center of gravity of steel beam
i Radius of gyration
L Span of composite beam
δ Plate-Thickness
λ Effective width measured on one side of the plane of symmetry
σ Stress
ν Poison's ratio

1. Introduction

The effective slab width is a concept used in flexural analysis of concrete T-beams and concrete-steel composite beams to simplify the computation of flange bending stresses. In order to determine the ultimate moment capacity of composite beams, the ultimate stress in the effective flange width is needed. Design calculations for composite beams are based on the theoretical concept of the *effective* slab width and not the actual width, or the spacing between T-beams. Due to the shear strain in the plane of the slab, the parts of the slab remote from the steel beam lag behind those in its proximity. This shear lag effect causes a non-uniform stress distribution across the width of the slab. The transmission of shear from the studs, welded to the top flange of the steel beam, to the concrete slab becomes less effective as the beam spacing, b_s, increases. Figure 1 shows a reduced effective value of slab width, b_e, which is used in design such that the area GHJK equals the area ACDEF (Johnson, 1975).

Several provisions have been provided by various design codes and other research studies. In comparison with available experimental data, code equations are conservative and empirical. Moreover, the accuracy in calculating the effective flange width has a pronounced effect on the computed ultimate moment and serviceability limit states, such as deflection, fatigue, and overloading. Therefore, there is clearly room to improve the computation of the effective flange width. The purpose of this paper is to evaluate the effective flange width of composite beams at various limit states and develop provisions for the computation of effective slab width using a more rational approach. The objectives of this research are to investigate analytically and experimentally the actual stress distribution in composite beams and the effect of the partial shear connectivity on the effective flange width. The experimental program aimed at validating the finite element model consists of eight beam specimens tested to failure. A parametric study is presented and the results are compared.

2. Previous Research Work

Schule (1909), Bortsch (1921), and Karman (1923) were the first to initiate the theoretical and experimental work on finding the effective flange width. Metzer (1929) and Miller (1929) extended von Karman's approach to solve the case of a single T-beam with infinite flange width subjected to a concentrated load at midspan. Their derived equation was given as follows:

$$\lambda = \frac{F}{2\delta\,[(h/i)^2 - 1]} \tag{1}$$

It was demonstrated that when the width-to-span ratio, b_s/L, is small, the effective width, 2λ (as was shown in Fig. 1) approximately equals the flange width b_s of the beam.

Adekola (1961) and Mackey *et al*. (1961) performed further analytical studies and took into account various parameters related to geometry and material properties. Only full composite action and elastic behavior were considered. Lee (1962) derived equations to analyze beam and slab combinations based on full composite action between the slab and the beam. Yam and Chapman (1968) reported that the two major factors affecting the effective width are the ratio of beam spacing to span length and the type of loading. Research based on elastic theory has shown that the ratio b_e/b_s depends on the ratio b_s/L and boundary conditions at the supports. Moreover, (Fahmy 1985) analyzed composite beams using a combination of the finite difference and the layered finite element methods, accommodating partial interaction. The study concluded that the effective slab width depends on the type of loading, and that the effective flange width increases with an increase in the degree of interaction.

Timoshenko and Goodier (1970) developed an equation which was based on the elementary bending theory. They introduced the effective flange width λ, such that the stress calculations applied to the transformed beam cross-section would yield the correct value of maximum bending stresses (Fig. 1). For example, by assuming a simple cosine function for the bending moment, $M = M_1 \cos(\pi\, x/l)$, the equation becomes as follows:

$$2\lambda = \frac{2L}{\pi\,(3 + 2\nu - \nu^2)} \tag{2}$$

The Journal of Engineering Research Vol. 8 No. 1 (2011) 28-43

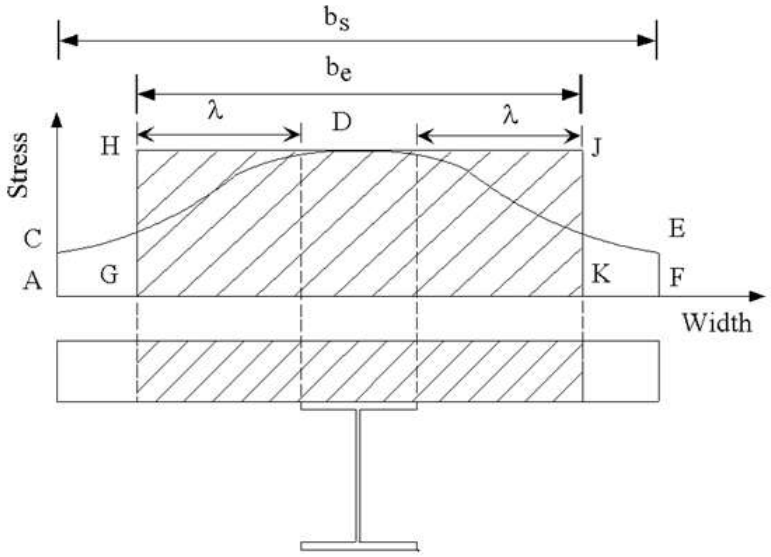

Figure 1. Stress distribution across the width of the concentrate slab

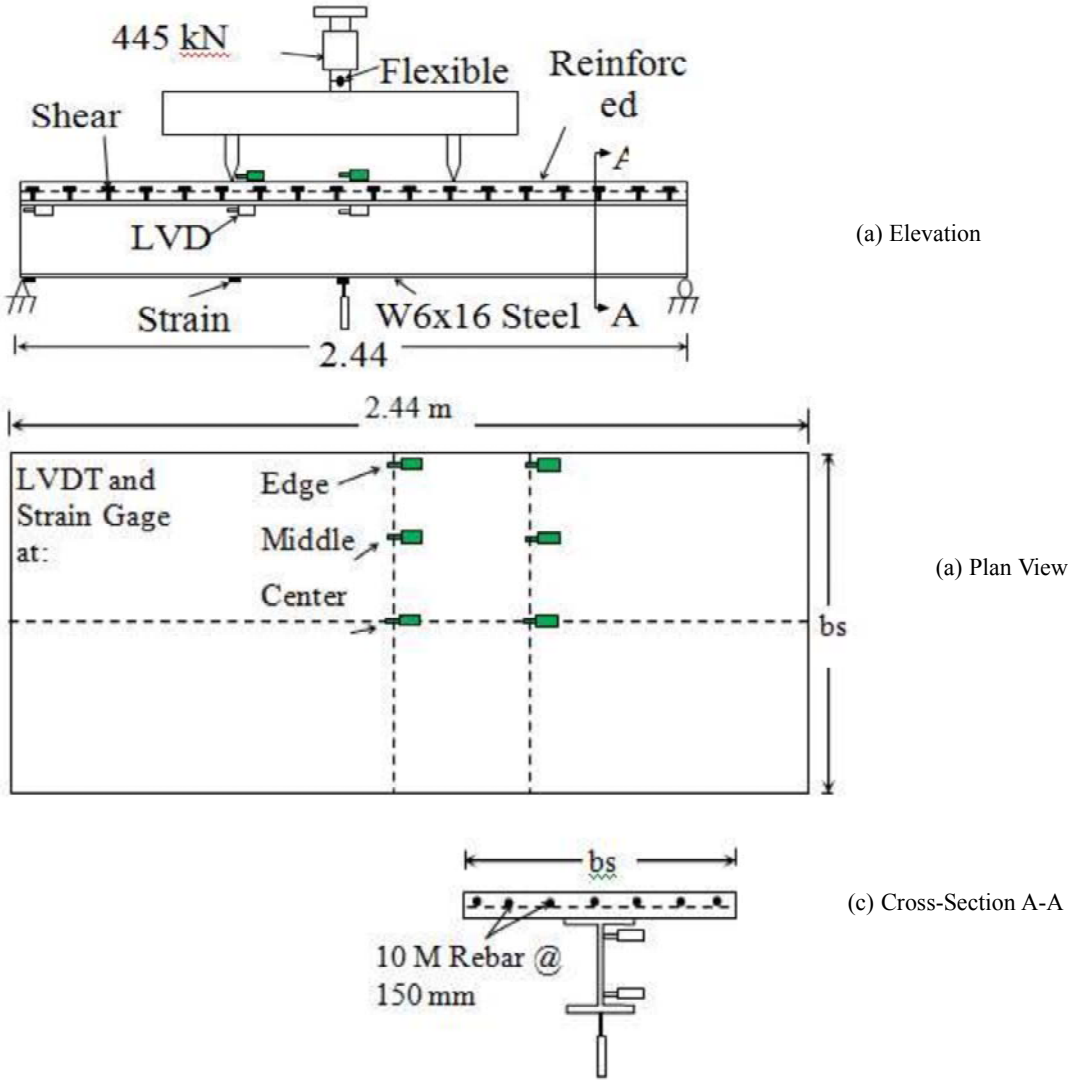

(a) Elevation

(a) Plan View

(c) Cross-Section A-A

Figure 2. Experimental setup and location of LVDTs, electrical strain gages, and load cell on beam specimen

The Journal of Engineering Research Vol. 8 No. 1 (2011) 28-43

Table 1. Formulate for effective widths in various design codes

Code	Formulae
AISC-LRFD: I3.1	b_e is least of (1) *L/4* (2) b_s (3) 2 times distance to edge of slab
CANADIAN CSA: S17.4 & Euro-Code (2000)	b_e is least of: (1) *L/4* (2) b_s

Table 2. Summary of experimental beams tested

Beam	Span Width (mm)	b_s / *L* ratio	Shear Connectors Percentage	Steel Beam Size
B1	610	0.25	100	W150x24
B2	864	0.35	100	W150x24
B3	1118	0.46	100	W150x24
B4	1118	0.46	75	W150x24
B5	1118	0.46	50	W150x24
B6	610	0.25	100	W150x13.5
B7	864	0.35	100	W150x13.5
B8	1118	0.46	100	W150x13.5

Table 3. Comparison of experimental and analytical results for all beams using various approaches to calculate b_s / b_s

Approach to calculate b_e/b_s					I	II	III	IV	V
Specimen	Shear Studs[c]	b_s (mm)	b_s/L	Exp.	NA	FEM Free Edge	FEM Edge Restraint	AISC	Eq. (6)
B1[a]	100%	610	0.25	0.981	0.998	1.00	1.00	1.00	1.00
B2[a]	100%	864	0.33	0.966	0.952	0.986	0.993	0.706	0.835
B3[a]	100%	1118	0.46	0.951	0.928	0.975	0.981	0.545	0.770
B4[a]	75%	1118	0.46	0.771	Slip	0.791	0.859	0.545	0.770
B5[a]	50%	1118	0.46	0.683	Slip	0.680	0.760	0.545	0.770
B6[b]	100%	610	0.25	-	0.995	0.996	1.00	1.00	1.00
B7[b]	100%	864	0.33	-	0.971	0.967	0.971	0.706	0.835
B8[b]	100%	1118	0.46	-	0.963	0.944	0.951	0.545	0.770

The Journal of Engineering Research Vol. 8 No. 1 (2011) 28-43

Recently, (Nassif *et al*. 2005 and Chen *et al*. 2007) have introduced equations that are based on experimentation and finite element modeling to determine the sensitive parameters influencing the effective flange width for bridges. Nassif *el al*. (2005) work included field testing of a continuous composite steel-concrete bridge as well as analysis of steel-box girders. The work focused on bridges and did not cover criteria for building.

3. Code Provisions

Most codes and design specifications have adopted methods for the computation of the ultimate moment capacity using the effective flange width concept. Table 1 shows the AISC-LRFD Design Specifications (2001), section I3.1, the Canadian Standards Association S16-01 (2001), section 17.4, and the Euro Code 4 (2002). The two North-American codes and EC-2000 are very similar where the length, *L*, is considered to be one of the most important parameters defining the effective flange width.

The code provisions simplify the specifications for be for practical reasons, however, these provisions have not changed over the last four decades. With the advancement of computer-based analysis and the introduction of high performance material such as high performance steel and high strength concrete, it is necessary to re-evaluate these provisions. Various approaches are applied in this paper using experimental and analytical methods to derive a new simplified equation that would take into consideration the sensitive parameters affecting the effective flange width of composite beams.

4. Experimental Program

The objective of the experimental program presented herein is to evaluate the effective width in steel composite beams having variable slab widths and different degrees of composite action. The experimental program consists of casting and testing eight composite steel beam specimens. Three parameters were considered: (1) the concrete slab width, (2) the percentage of shear connectors, and (3) the steel beam section. All the tested beams had the same span length of 2.44 m, concrete strength of 36 MPa, and steel beam yield strength of 354 MPa. From Table 2, the first set of beams B1, B2, and B3 have varying span widths. Beams B3, B4 and B5 vary in shear connector percentages as compared to fully connected composite beams. Beams B6, B7 and B8 also have varying span widths but the steel I-beam is smaller in size than the previous beams. The steel beam size for Beams B1 through B5 is W150x24 (W6x16), while for Beams B6 through B8 the size is W150x13.5 (W6x9).

Figure 2(a) shows the setup for testing the specimens under a two point loading system. The setup consists of a two point loading steel frame, a load cell of 445 kN, LVDT with a measuring range of ± 152 mm, and strain gages. Figure 2(b) shows the top view of the beam, location of the strain gages and LVDT's used to measure strain in the concrete. Similar configuration was at the bottom fibers of the concrete slab. Figure 2(c) shows a cross-section of the beam, the rebar, the vertical LVDT used to measure deflection, and the horizontal LVDT's used to check for rotation and lateral movement out-of-plane of the steel beam.

A 48-channel data acquisition system was used to collect data from 34 strain foil gages, one load cell, and 12 LVDT's (50 mm measuring limit) were used to measure the concrete strain at the top and bottom of the composite beam's concrete slab. The concrete strain at the top of the composite beam location was measured using six strain gages and six LVDT's at each location. They were placed across the middle section of the beam and next to the applied load. Similar configuration (six LVDT's and six strain gages) was also placed at the bottom surface of the concrete slab as shown in Fig. 2(b).

All beam specimens were built and cast at the Rutgers University Structural laboratory, however, the steel beams were transported to a professional welding shop where a specialized technician welded the shear studs. The shear studs spacing was determined according to the AISC-LRFD specifications for the first and third set of beams. Afterwards the beams were transported back to the laboratory where the formwork and reinforcing steel were prepared and finalized. A strain gage installation was also performed for all five beams. The beams were cast using commercially available, local, ready mixed concrete to ensure uniformity of concrete strength in the flanges. All beams were left to cure under room temperature. Subsequently, the beams were loaded to failure using a constant loading rate and on the day of testing, four control cylinders having embedded strain gages were tested to obtain the concrete strength and its stress-strain relationship.

5. Finite Element Models

The Finite Element (FE) method of analysis was used to evaluate the exact distribution of stresses in the concrete deck slab for simply supported beams. The finite element program ABAQUS, which was used in the analysis provides for concrete and steel constitutive material models, as well as reinforcement in the

The Journal of Engineering Research Vol. 8 No. 1 (2011) 28-43

concrete slab and shear connectors for the composite action. The material models were verified using results from tests performed in this study as well as by other researchers, namely, (Robinson, Wallace 1973 and Fisher 1974).

Two- and three-dimensional FE models with various types of elements were develop. The analysis was carried out using three different types of elements: beam, shell, and solid elements. Utilizing these elements, three different FE models were developed. The beam-beam (B-B) model had both the slab and steel beam represented by 2-noded beam elements connected by "Beam" type MPC acting as a rigid link between the nodes of the concrete slab and the corresponding nodes of the steel beam. The shell-beam (S-B) model had the concrete slab represented as a 4-noded, two-dimensional shell elements, and the steel beam by as 2-noded beam elements. The two types of elements were connected using a "Beam" type MPC also. Figure 3(a) and (b) illustrates the solid-solid (S-S) model having 8-noded, three-dimensional brick elements representing the concrete slab and steel beam. A convergence study was performed to evaluate the accuracy of having 2 layers of solid elements through the depth of the concrete slab, versus 3 and 4 layers. A comparison of the three models, presented in Fig. 4(a), shows that the results are very similar for all three models. It was concluded that the three models gave very similar results, therefore the 2 layer model was since it needed less time and memory to run. The interface between the concrete flange and beam elements is represented by a "TIE" type MPC, which makes all active degrees of freedom equal at each of the two "tied" nodes. The disadvantage of the beam-beam model is that it does not provide the transverse strain distribution in the concrete flange section. The solid-solid model was used in the final analysis since it provided the cracking pattern and allowed for representation of shear studs. Figure 3(d), (e) and (f) show the displaced shape as well as the contour plot of the composite beam at 3 various loading levels, where it is observed that stresses at the middle of the beam are highest and decreases towards the edge of the concrete slab.

The concrete material model consists of an isotropically hardening yield surface, and has an independent "crack detection surface" which determines if a point has failed by cracking. To illustrate the crack orientation and pattern, ABAQUS/Explicit was utilized besides ABAQUS/Standard. Two constitutive models are used for the analysis of concrete: (1) a brittle cracking model and (2) a damaged plasticity model. The fracture strength of the concrete given by the ACI 318-32 Code (2002) was calculated from the compressive strength of the concrete using the equation $f_r = 7.5 \sqrt{f_c'}$. From this value the cracking stress of concrete is determined, and the elastic-plastic curve is obtained. The brittle cracking model is defined using the brittle cracking and brittle shear options. ABAQUS/Explicit was also used to model partial interaction (shear connectors) between concrete slab and steel beam using "spot welds" option. The rebar option with the measured stress-strain model was used for the steel reinforcement in the concrete. The interaction between the reinforcing steel and concrete is also considered by introducing tension-stiffening into the concrete cracking model, which simulates load transfer across cracks through the rebar. The measured stress-strain relationship for steel beam was also used in the models. However, in the composite beam, the steel beam does not go beyond its ultimate strength due to the fact that the concrete slab has reached its ultimate strength earlier than that of the steel beam.

Due to its symmetry, only half of the beam was modeled by having a symmetry boundary condition applied at the mid section. Another boundary condition was imposed at the end of the bottom steel flange, simulating a simply supported beam. The analysis was performed by applying an incremental load with iterations to obtain force and moment equilibrium in each increment, using the RIKS algorithm. This approach determines the static equilibrium solution for unstable response in concrete due to cracking in tension, yielding of reinforcement, or concrete softening in compression.

6. Model Validation

The analytical Solid-Solid FE model was compared to results from a number of tests to demonstrate its validity and accuracy. Robinson and Wallace (1973) tested simply supported composite beams having a span length of 6.4 m, loaded at midpoint. They consisted of a steel beam type W12x19, a slab thickness of 102-mm, and a slab width of 1727-mm. The steel strength (F_y) was 345 MPa and the concrete strength (f_c') was 35 MPa . A minimum steel reinforcement of welded wire mesh was used in the middle of the solid concrete slab. The shear connectors were 95% for B1 and 53% for B2 of the total number required by design. The loading for beam B1 and B2 (Robinson and Wallace, 1973) considered was applied at mid-span until failure. Moreover, Fisher (1974) tested a simply supported composite beam having a span length of 5.6 m, under a two-point loading where each load was 0.3 m from midpoint. The beam was made up of a W12x27 steel section, and a slab width and thickness of 140 mm and 1.22 m, respectively. The steel strength (F_y) was 248 MPa and the concrete strength (f_c') was 27.5 MPa. The steel reinforcement was number 15 M rebar with a grid of 0.2 m by 0.2 m.

The Journal of Engineering Research Vol. 8 No. 1 (2011) 28-43

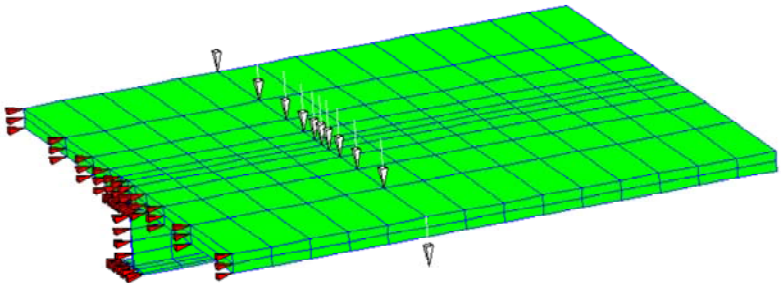

(a) Solid-Solid Model

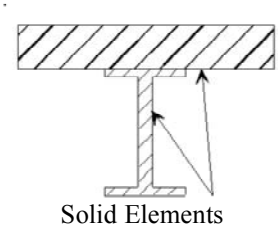

(b) Schematic of S-S Model

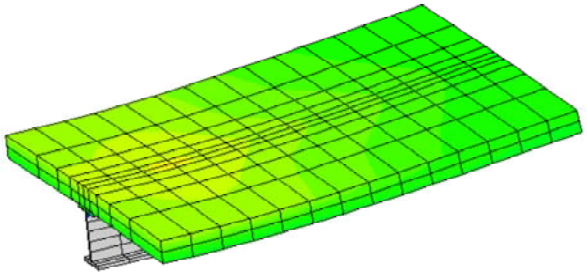

(c) At 30% of Ultimate Load

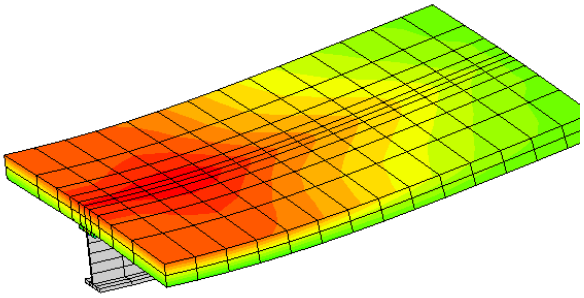

(d) At Cracking

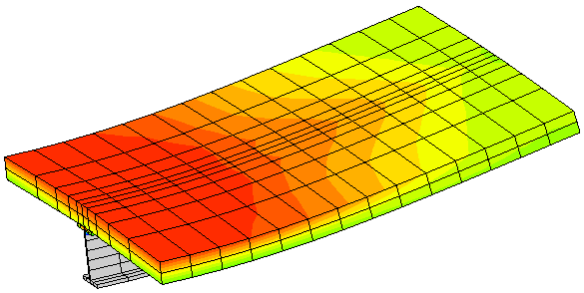

(e) At 90% of Ultimate Load

Figure 3. 3-D view of the composite beam solid-solid model; the stress distribution and the deformed shapes are shown in (c), (d) and (e)

The Journal of Engineering Research Vol. 8 No. 1 (2011) 28-43

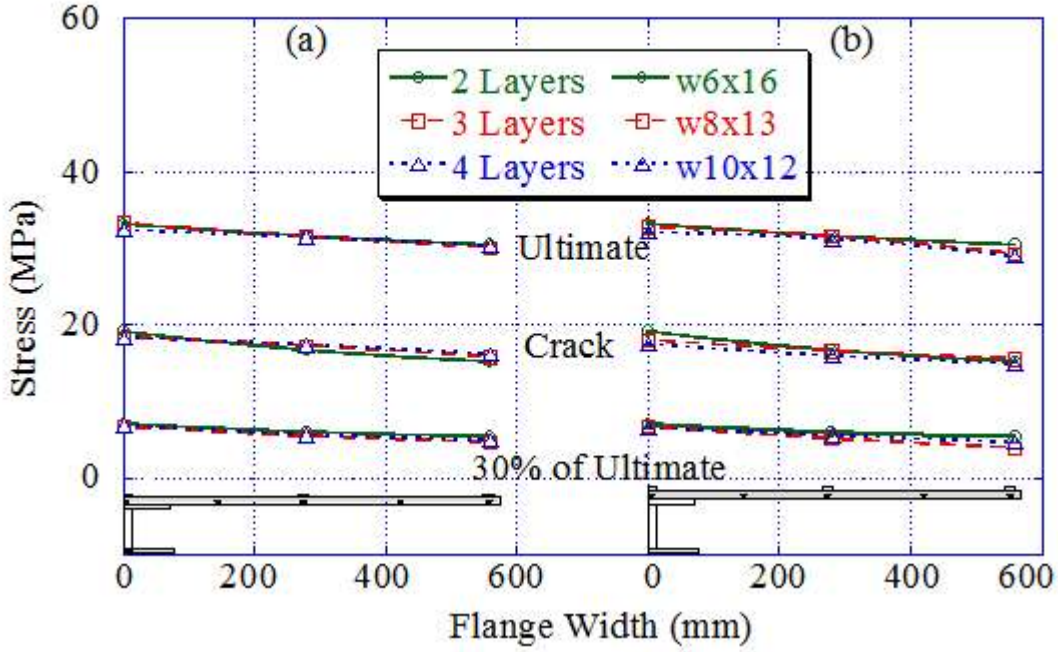

Figure 4. Comparison of stress distribution for composite beams with (a) varying mesh layers and (b) varying steel beam sections

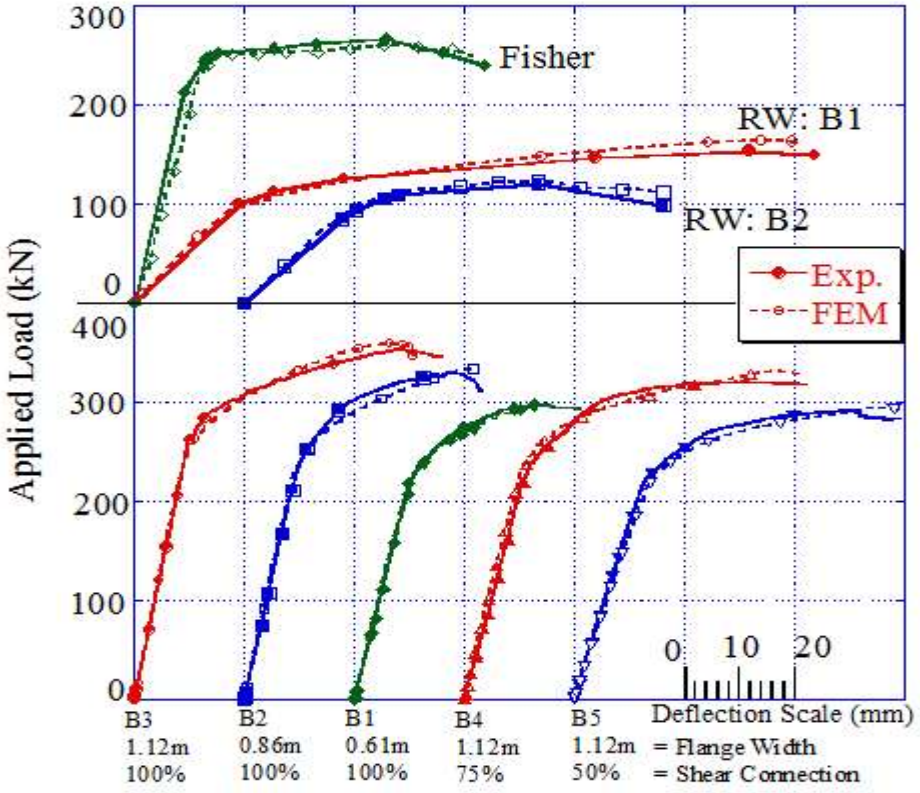

Figure 5. Relationship of experimental and FEM applied load versus midspan deflection

The Journal of Engineering Research Vol. 8 No. 1 (2011) 28-43

The shear connectors were 95% of the total number allowed by design.

Figure 5 shows comparison between experimental data and those obtained from the model. The figure shows both sources of beam tests used to validate the FE model developed in this study. The model exhibits very good agreement with the experimental results at various load levels. At ultimate load, the percentage difference is 4% for the Robinson and Wallace's beams, 3% for Fisher's beam, and 3% for beams B1 through B5. Additionally, the strains in the concrete slab obtained from measurement instruments (LVDT and strain gage) and FE model were compared. Figure 6 shows a comparison between the experimental strain measurements and the analytical results using FEM at two locations: along the centerline of the beam (center) and near the edge of the slab. Results shown in Fig. 6 suggest that the FE model is very accurate in predicting the longitudinal strain distribution over the width of the slab.

Figure 7 displays the cracking pattern of the beam, which was initiated at the bottom fibers of the concrete slab underneath the load, in comparison to that obtained from the FE model solved in ABAQUS/Explicit. There is a very good agreement between the expected cracking pattern and its actual location. From the results presented, it was concluded that the finite element (solid-solid) model predicted the behavior of the composite beams and can be used in the parametric study.

7. Effective Flange Width Determination

Four different approaches were utilized to determine the effective flange width for the beam specimens. Each approach is discussed and compared to the experimental results. The stress at various loading stages was determined using the measured strain across the width of the concrete flange and the measured concrete stress-strain relationship. The area under the stress distribution curve ACDEF, shown in Fig. 1, was then determined and divided by the maximum stress value. The effective slab width is given as follows:

$$b_e = \frac{A}{\sigma_{y\max}} \tag{3}$$

where A is the area under the stress distribution curve, and $\sigma_{y\ max}$ is the maximum longitudinal stress across the flange width occurring at the midpoint above the web. Table 3 presents the final results for the ratio of b_e / b_s using various approaches.

Approach I was used to determine b_e by applying the equilibrium equations for forces and moments and by the neutral axis location, which is known from the measured strains in the beam. The applied external moment is equated to the internal resisting moment, due to the forces acting on the cross-section of the composite beam. Figure 8 shows the strain and stress distribution over the depth of the cross-section of a typical beam. Figure 8(a) displays the strain values obtained from the experimental data. The strain values demonstrates that in the elastic range the neutral axis is located at the bottom of the top steel flange, as shown in Fig. 8(b), and shifts upwards to be within the top steel flange at ultimate loads, as shown in Fig. 8(c). The stress values are then determined using the constitutive stress-strain relationships obtained experimentally for concrete and structural steel, respectively. Since b_e is calculated at ultimate load, Fig. 8(c) is used to calculate the internal moments. For example, the force value at the steel beam's bottom flange was calculated as follows:

$$T_{BF} = A_{BF}\sigma_{BF} \tag{4}$$

where A_{BF} is the area of the bottom flange and σ_{BF} the stress value acting on that area. For two-point loading, the maximum external moment, M_{ext}, is given by $M_{ext} = PL/6$, where P is the ultimate value of loading obtained experimentally, and L is the length of the beam. Then, equating both, external and the internal moments, $M_{ext} = M_{int}$, b_e, be can be expressed as:

$$b_e = \frac{M_{ext} + T_W a + T_{TF} b - C_{TF} c - C_{As} d}{\sigma_{conc} t_s e} \tag{5}$$

Approaches II and III to calculate b_e/b_s were performed using the area under the stress curve over the width of the concrete slab, by getting the exact value of stress at each element across the width of the concrete flange, as illustrated previously in Fig. 3. Using the Solid-Solid finite element model described earlier, the stress at any element and therefore the stress distribution at the top concrete fibers was determined. Approach II, like the experimental beams, had no constraints at the concrete slab edges, while Approach III had lateral and moment constraints to simulate a continuous floor slab. It is observed from Table 3 that Approach II gives lower values of the ratio b_e / b_s therefore it is more critical than Approach III. Figure 9 illustrates the stress distribution in the flange of each beam at various loading levels: 1) 30% of ultimate, 2) cracking of concrete, and 3) 90% of ultimate. Experimentally, severe cracking of the concrete slab occurred at ultimate causing damages to the strain gages at that level, but the results were accurate up to 90% of ultimate; therefore the verification was performed up to 90% of ultimate, but the ultimate level

The Journal of Engineering Research Vol. 8 No. 1 (2011) 28-43

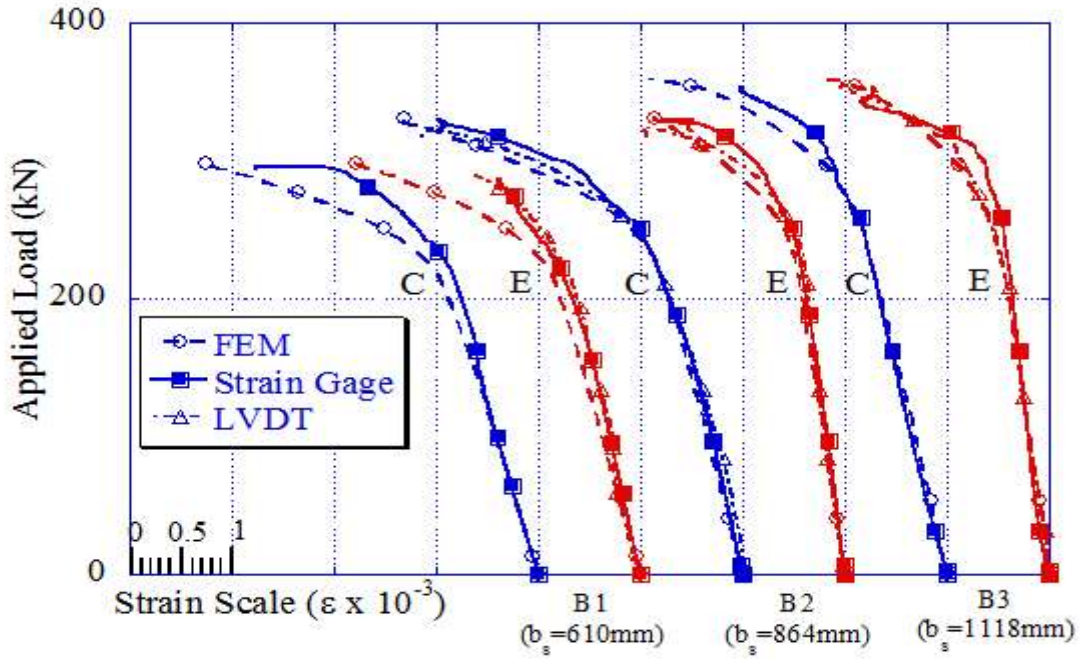

Figure 6. Comparison between FEM, strain gage, and LVDT strain results at middle of beam (C: center, E: Edge)

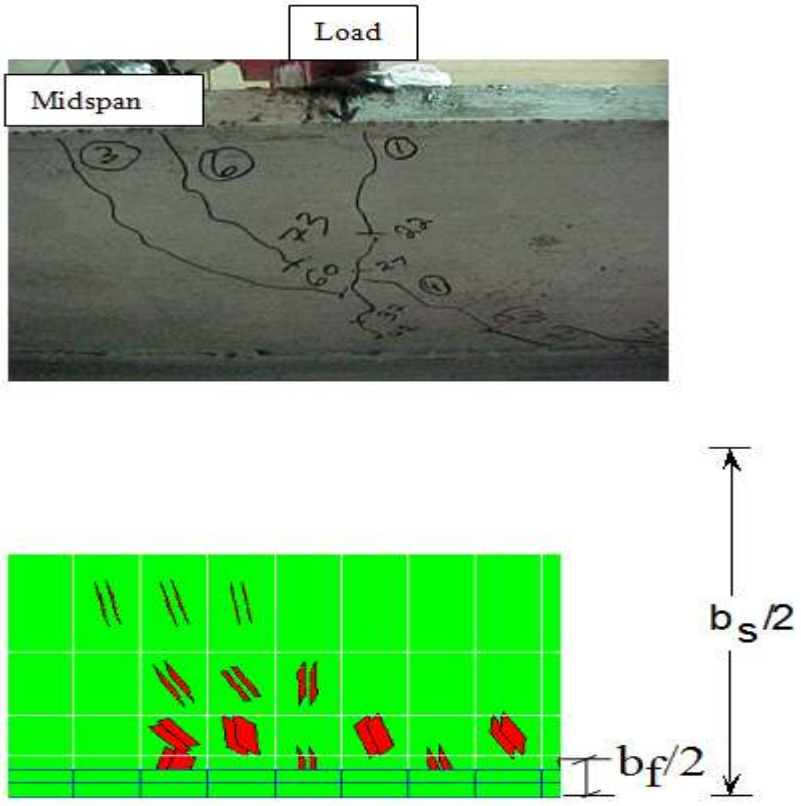

Figure 7. Comparison of experimental and FE results for cracking of concrete slab at bottom fibers

The Journal of Engineering Research Vol. 8 No. 1 (2011) 28-43

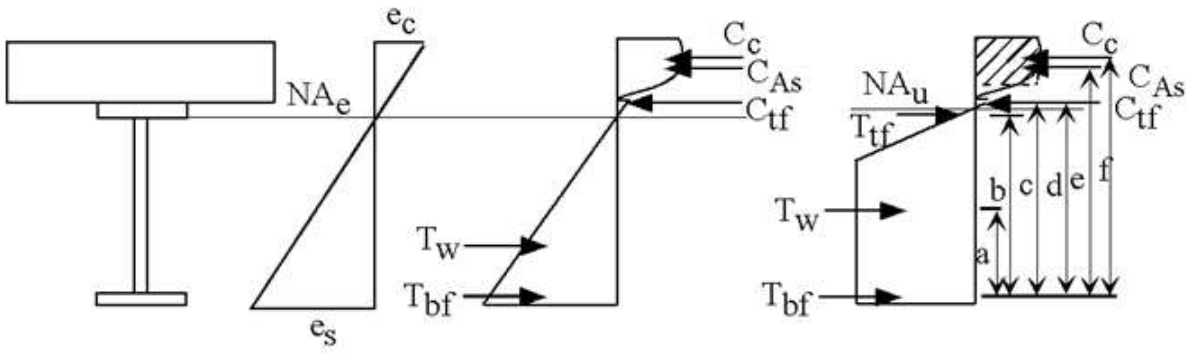

(a) Strain (b) Elastic Stress (Stress at Ultimate

Figure 8. Neutral axis position and stress distribution at various load levels

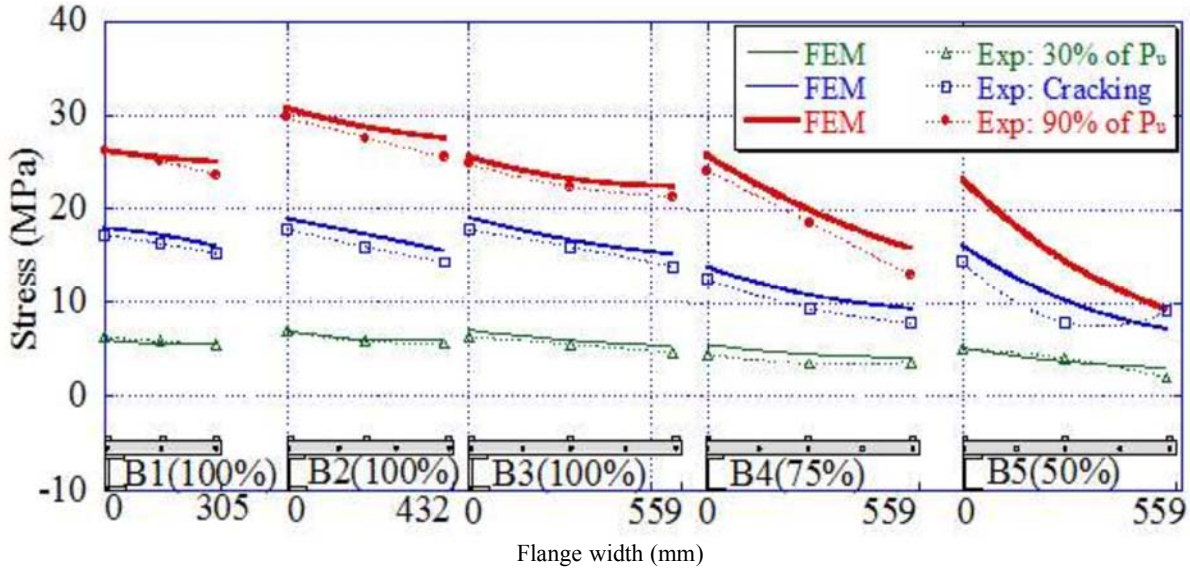

Figure 9. Variation of analytical and experimental stress width flange width at various load levels

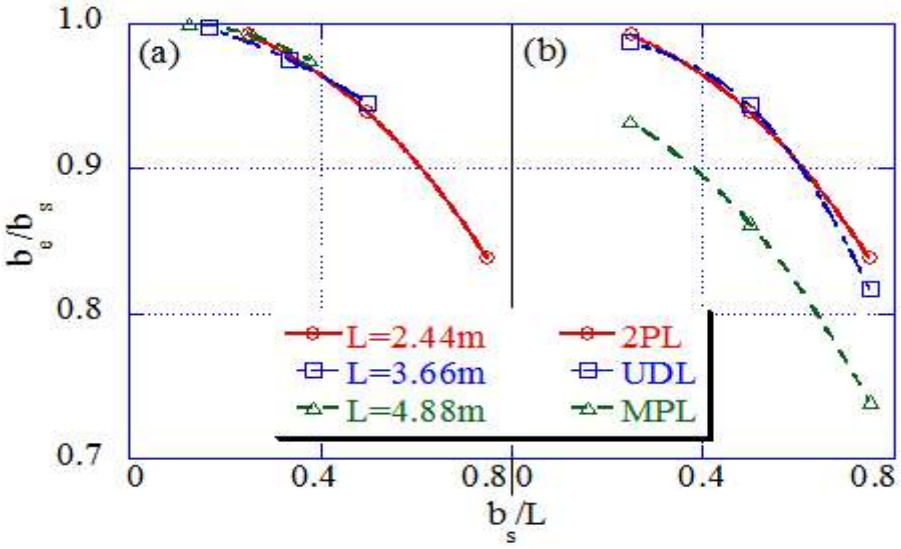

Figure 10. Relationship of b_e / L and b_s / L relationships for (a) various span lengths and (b) loading type

The Journal of Engineering Research Vol. 8 No. 1 (2011) 28-43

was chosen for the FEM parametric study. From Fig. 9 and using Equation (3), the ratio of b_e/b_s is calculated. It is observed that the first three approaches compare very well with the experimental results. It also shows that as the width of the flange (b_s) increases, the b_e/b_s ratio decreases.

From the experimental results as well as Approach II, the ratio of b_e / b_S decreases by 19% and 28% for Beams B4 and B5 as compared to beam B3, respectively. Shear connectors are therefore a significant parameter affecting b_e. Moreover, since the experimental and FE model results are very similar, it is concluded that the design requirements for shear connectors specified by the AISC-LRFD code are satisfactory. And since the design of composite beams assumes full interaction, it is important to design for the correct number of shear connectors and to strictly insure that this is upheld in the actual construction.

It is observed that there is little difference of b_e for beams B6, B7, and B8. This is due to the fact the neutral axis of the composite beam was actually within the concrete slab, whereas for the other beams (B1, B2 and B3) with a larger steel section, the neutral axis was within the top flange of the steel beam. Therefore, the concrete fibers below the neutral axis were in tension rather than compression, causing only the top fibers of the concrete slab to be under compression where the most the concrete flange became effective. Since not all the depth of the concrete section was utilized, the stress in the concrete across the width of the slab did not vary much for the three beams.

Approach IV, to find b_e / b_s, was performed by applying the code provisions specified by the AISC. It is observed that there is a decrease of 37% and 74% in b_e / b_s ratio for beams B2 and B3 using the experimental results as compared to the AISC specifications, respectively. It is concluded that the code requirements to obtain be are conservative.

8. Parametric Study

With an FE model that accurately predicts the behavior of the beam, a parametric study is performed using 41 cases. The parameters studied were the slab width, b_s, the span length of the beam, L, the thickness of the slab, t_s, width of the steel flange, b_f, concrete strength fc', the steel beam strength F_y, loading type, and shear connector percentage. A total of nine variations for each parameter was analyzed.

It was concluded that the only parameters that significantly influenced b_e were the b_s, L, and load type. Fig. 10(a) show the relationship between b_e / b_s versus b_s / L for three sets of curves, such that each set had three beams of constant length of 2.44 m, 3.66 m and 4.88 m. Within each set, the width of the slab varied; 610 mm, 1219 mm, and 1830 mm for each beam. The loading applied was a two-point loading. It is observed that with an increase of b_s / L from 0.25 to 0.75, b_e / b_s decreases by 15%.

Figure 10(b) also present three sets of beams with varying load types: two-point loading (2PL), midpoint loading (MPL), and uniformly distributed loading (UDL). Within each set, the slab width varied; 610 mm, 12190 mm, and 1830 mm for each beam. The span length was kept constant for all the beams at 2.44 m. It is observed that the ratio b_e / b_s does not significantly change for 2PL and UDL, however an average decrease of 6% for the b_e / b_s occurs for the load type MPL as compared to 2PL. It is concluded that 2PL and UDL have similar effect on the effective flange width, while MPL decreases b_e in contrast to the other types of loading. Since uniformly distributed loading is the common type of loading acting on structural beams, evaluating b_e using two-point loading would be more accurate than using mid-point loading.

From the experimental results, it is observed that the percentage of shear connectors also affect b_e. From Figs. 11 and 12, as the percentage of shear connectors decrease so does the effective flange width. It is also observed from Fig. 11 that b_e increases for the fully connected beam, B3, with a higher load, while b_e decreases for beams with lower shear connectors. The decrease in b_e as the percentage of shear connectors decrease indicates that the concrete slab is slipping at the interface with respect to the steel beam at various loading levels, as illustrated in Fig. 12. Therefore, it is concluded that partial interaction adversely affects b_e and the code requirements for the design of shear connectors are satisfactory to achieve complete interaction preventing shear slip.

A parametric study was also performed to investigate the effect of the steel beam depth on b_e. The composite beams were designed such that the concrete slab and the moment capacity of the beams were kept the same. The steel beams used were w6x16, w8x15 and w10x17. From Fig. 4(b), it was observed that the stress distribution for the three beams did not change as the depth increased. Concluding that the steel beam depth is not an effective parameter in calculating the effective flange width.

9. Comparison of Results

From the parametric study performed, the most significant relationship affecting b_e is b_e / b_s versus b_s / L. Figure 13 plots b_e / b_s versus b_s / L ratios for the analytical curves 30% of ultimate, cracking of concrete and at ultimate load capacity compared to AISC-

The Journal of Engineering Research Vol. 8 No. 1 (2011) 28-43

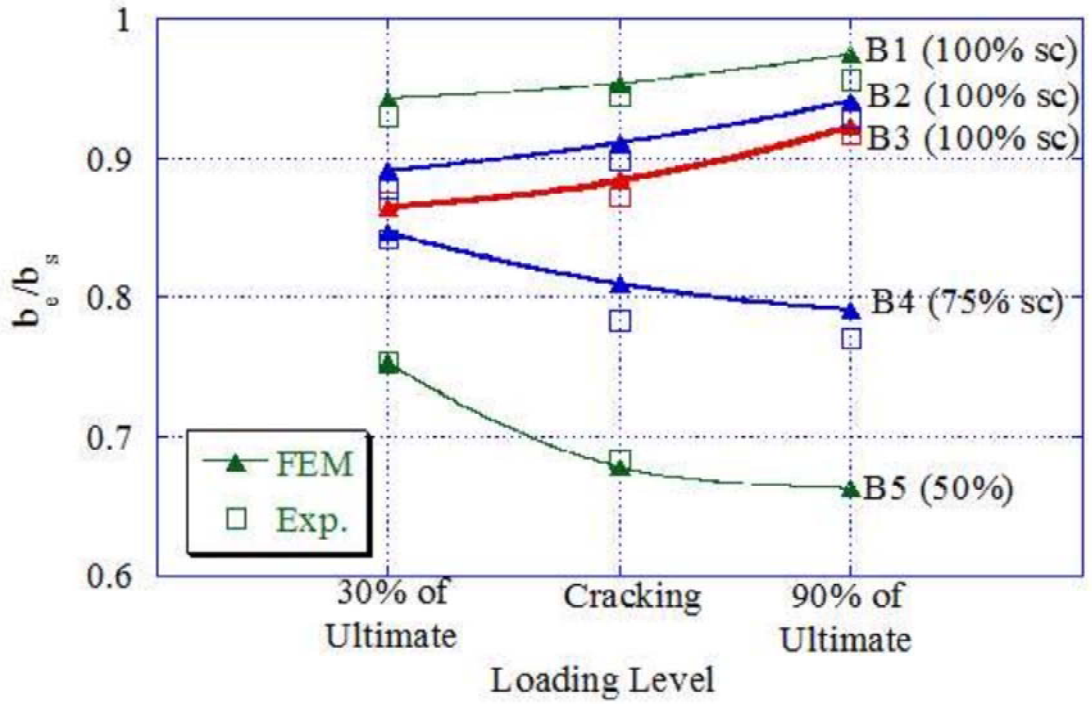

Figure 11. FEM and experimental b_e / b_s at increasing loading level for B1 and through B5 at 30% of ultimate load, cracking of concrete slab, and 890% of ultimate load

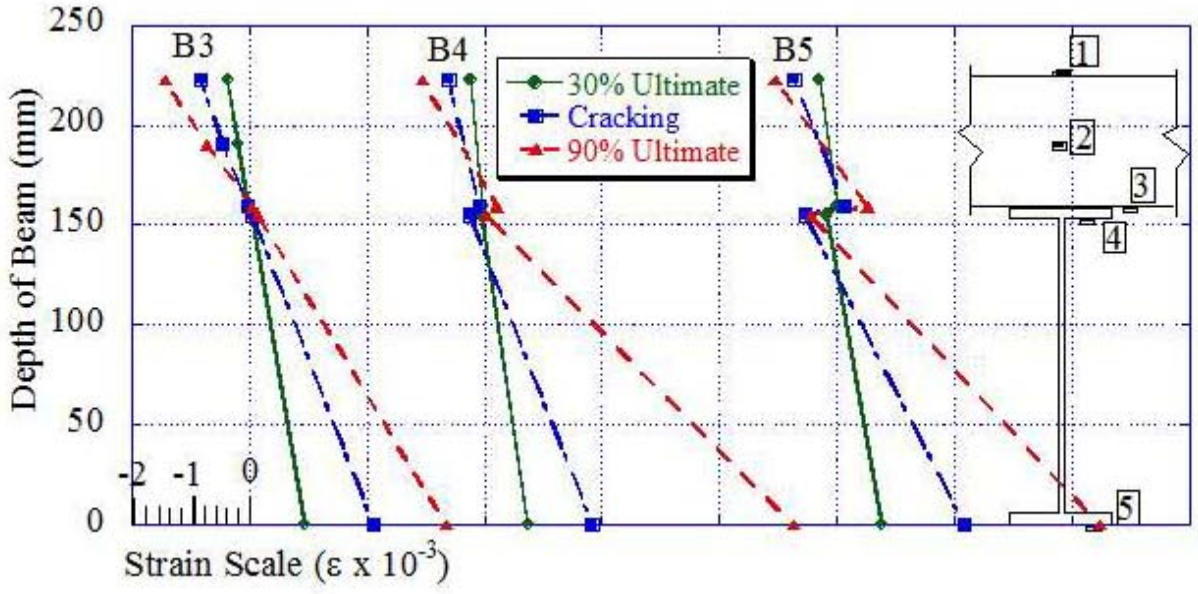

Figure 12. Shear slip for beams B3, B4, and B5 at various loading levels

The Journal of Engineering Research Vol. 8 No. 1 (2011) 28-43

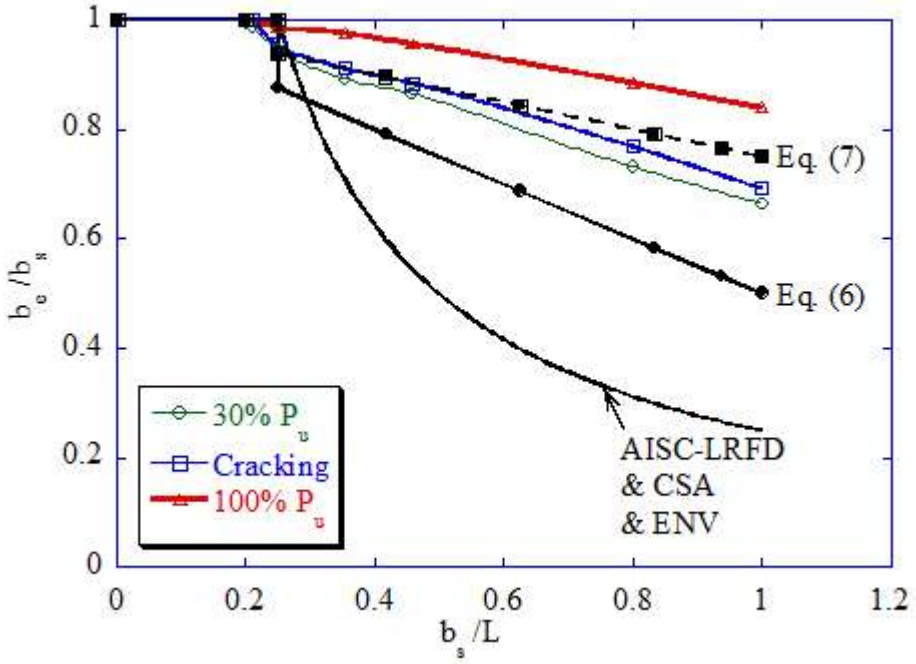

Figure 13. Comparison of methods for determination of effective width using b_e / b_s versus b_s / L

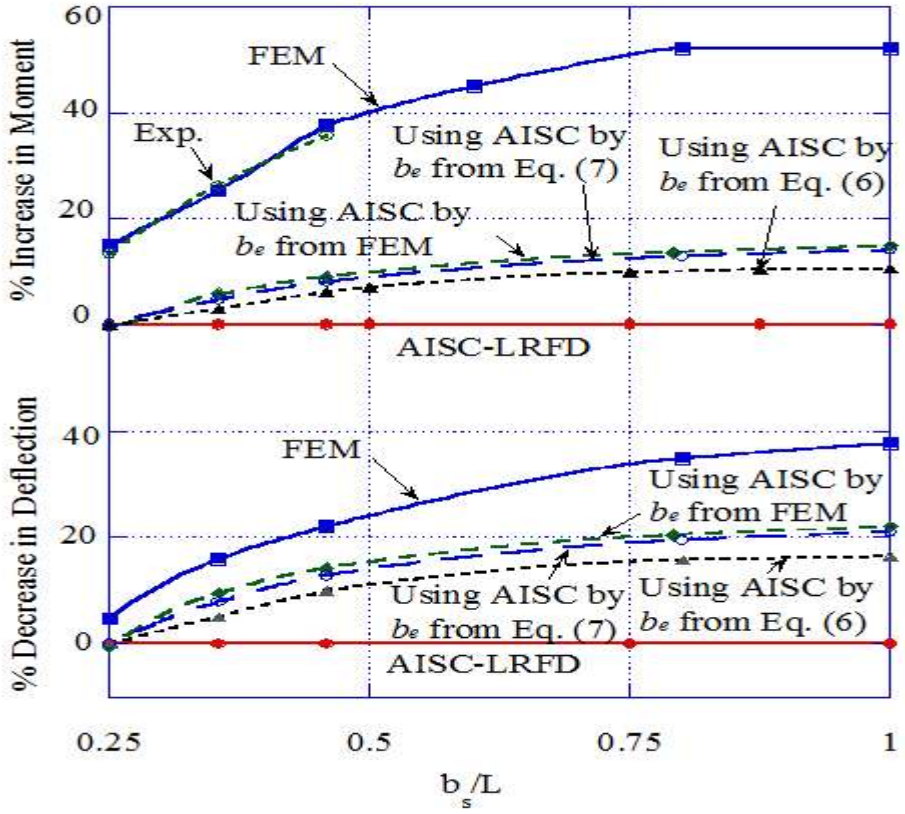

Figure 14. Percentage diffrerence in moment capacity and deflection due to implementation of proposed equation

The Journal of Engineering Research Vol. 8 No. 1 (2011) 28-43

LRFD code values. It is observed that the FEM curves are all higher than that of the AISC-LRFD curve. At b_s / L of 0.35, for example, the percentage difference for b_e / b_s ratio between the ultimate and the code's values is 50%. Moreover, it is observed that the Canadian and European Codes give the same curves as AISC-LRFD Code. It is noted that b_s / L is the main ratio that affects the b_e / b_s ratio significantly. This is observed by the experimental and FEM analysis results, by the codes values, and by the conclusion of the results of a number of previous research. Even though the other parameters studied affect the load carrying capacity of the composite beam, but they did not significantly affect b_e. Using the curves developed in Fig. 13, a trend is observed such that the curves obtained through this research resemble a straight line. To account for the difference between the FEM (and experimental) curves at serviceability and at ultimate, an equation for each loading level is recommended. The equation for b_e at serviceability is

$$b_e / b_s = 1 - 0.5\left(\frac{b_s}{L}\right) \qquad \text{for } b_s / L > 0.25 \qquad (6)$$

and at ultimate

$$b_e / b_s = 1 - 0.25\left(\frac{b_s}{L}\right) \qquad \text{for } b_s / L > 0.25 \qquad (7)$$

where $b_e = b_s$ for $b_s / L \leq 0.25$. From Table 3, the ratio of b_e / b_s at ultimate, as obtained by the Eq. (6) compares better to the experimental results as compared to the AISC values. As observed from Fig. 13, the proposed equation's curves fall just below the FEM curves for each loading level. The advantage of the equations is that it is simple to use, is closer to the experimental results than code values, takes into consideration the sensitive parameters that affect b_e, and utilizes more of the section moment capacity needed for ultimate load design of up to 10%, as illustrated in Fig. 14. The equation also affects the service limit states of the beam, where the moment capacity increases up to 14% and deflection decreases down to 20% (Fig. 14). The AISC-LRFD provisions are conservative with an effective flange width value that underestimates the stiffness.

10. Conclusions

A study of the effective flange widths for composite beams was presented. An experimental as well as a finite element analysis was used in the investigation. The modeling of the composite beam was made up of 3-D solid elements incorporating the material properties of the different components of the composite beam. From this research, a number of conclusions were drawn:

1. The finite element model presented in this paper predicted well the behavior of the beam specimens tested in this and other research studies. Based on the FE model, it was found that the sensitive parameters affecting b_e are the span length, L, the slab width, b_s.
2. The number of shear connectors significantly affects the effective flange width. A reduction of shear connectors by 25% (beam B4) and 50% (beam B5) caused a decrease of 19% and 28% in b_e / b_s, respectively, as compared to the complete shear interaction specified by the design code of beam B3. Based on these results, the code requirements for shear connectors are considered satisfactory.
3. From the experimental and FEM results, the effective flange width used by the AISC-LRFD is conservative and is underestimated by up to 43% for beam B3, where the code provision ratio of b_e / b_s is 0.545 as compared to the experimental ratio of 0.951.
4. Based on the experimental and analytical work carried out in this study, robust simple equation, Eq. (7) for ultimate load level and (6) for serviceability limit state, are proposed to compute the effective flange width, where the b_e / b_s ratio using the equation is 0.770 for beam B3, an underestimated ratio of 19% only. Moreover, Fig. 14 shows that for ultimate load level, a gain in moment of 10% and a reduction in deflection of 14% could be achieved, and for serviceability limit state, a gain in moment of up to 14% and a reduction in deflection of up 20%, by using b_e obtained from the proposed equation as compared to the code's requirement. The effective flange width values obtained by these equations were proven to be more accurate and less conservative than the AISC-LRFD values. The equations presented in this paper are based on the experimental findings of a certain range of dimensions provided in Section 2 and Table 2. Further testing would be advantageous to explore the applicability of the developed equations to other set of ranges.

References

ABAQUS/Standard User's Manual, 2000, Version 6.1, Hibbitt, Karlsson & Sorensen, Inc.

ACI 318-02, 2002, "Building Code Requirements for Reinforced Concrete."

AISC, 2001, "Manual of Steel Construction: Load and Resistance Factor Design - Third Edition," American Institute of Steel Construction, Inc.

Abu-Amra, T., 2003, "Development of Effective Flange Width Criteria for Composite Steel Structures," Ph.D. Dissertation, Rutgers University, New Jersey, USA.

Adekola, A.O., 1961, "Effective Widths of Composite Beams of Steel and Concrete," The Structural Engineer, Vol. 16(9), pp. 285-289.

Bortsch, R., 1921, "Die Mitwirkende Plattenbreite (The Plate Width Contributors)," Der Bauingenieur (The Civil Engineer), Vol. 23, pp. 662 - 667 (in German).

Canadian Standards Association, 2001, S16-01, Limit State Design of Steel Structures.

Chen, S., Aref, A., Chiewanichakorn, M. and Ahn, I., 2007, "Proposed Effective Width Criteria for Composite Bridge Girders," Journal of Bridge Engineering, ASCE, Vol. 12(3), pp. 325 - 338.

Davies, C., 1975, "Steel-Concrete Composite Beams for Buildings," George Godwin Limited.

DD ENV, 2002, 1994-2:2001, "Eurocode 4: Design of Composite Steel and Concrete Structures," Part 2: Composite Bridges, British Standards.

Fahmy, E. H. and Robinson, H., 1985, "Effective Slab Widths for Simple Composite Beams with Ribbed Metal Deck," Modeling, Simulation & Control, B, AMSE Press, Vol. 3(1), pp.19-36.

Fisher, J. W., Kim, S.W. and Slutter, R.G., 1974, "Tests of Lightweight Concrete Composite Bridges at Ultimate Load," Civil Engineering Report, No. 54, Univ. of Maryland.

Hagood, T. A., Guthrie, L. and Hoadley, P. G.,1968, "An Investigation of the Effective Concrete Slab Width for Composite Construction," Engineering Journal, AISC, pp. 20-25.

Johnson, R. P., 1975, "Composite Structures of Steel and Concrete," Halsted Press, John Wiley & Sons.

Karman, T. v., 1923, "Festschrift August Foppls," International Association of Bridge Structural Engineering, pp.114.

Lee, J.A.N., 1962, "Effective Widths of Tee-Beams," The Structural Engineer, Vol. 40(1), pp. 21-27.

Mackey, S. and Wong, F.K.C., 1961, "Effective Width of Composite Tee-Beam Flange," The Structural Engineer, Vol. 39(9), pp. 277-285.

Metzer, W. v., 1929, "Die Mittragende Breite (The Loading Bearing Width)," Luftfahrtforschung (Aeronautics Research), Band 4 [in German].

Miller, A. B., 1929, "The Effective Width of a Plate Supported by a Beam," The Institution, London.

Nassif, H., Abu-Amra, T. F. and El-Tawil, S., 2005, "Effective Flange Width Criteria for Composite Steel Girder Bridges," Proceedings of the 84th Annual Meetings of Transportation Research Board, Paper No. 05-2477, Washington, D.C.

Robinson, H. and Wallace, I.W., 1973, "Composite Beams with 1 ½ inc Metal Deck and Partial and Full Shear Connection," Canadian Society for Civil Engineering, Vol. 16(A-8).

Schule, 1909, "Mitteilungen der Eidgenossischen Materialprufungsanstalt (Communications of the Swiss Federal Institute of Materialprufungsanstalt," Zurich (in German).

Timoshinko, S. and Goodier, J. N., 1970, "Theory of Elasticity," McGraw-Hill Co., New York.

Yam, L.C.P., and Chapman, J.C., 1968, "The Inelastic Behavior of Simply Supported Composite Beams of Steel and Concrete," Proceedings of the Institution of Civil Engineers, Vol. 41, Paper 7111, pp. 651-683.